Article:
Dreva, K, Morina, A, Yang, L orcid.org/0000-0003-0935-3921 et al. (1 more author) (2022) The effect of temperature on water desorption and oxide formation in MoS2 coatings and its impact on tribological properties. Surface and Coatings Technology, 433. 128077. ISSN 0257-8972

https://doi.org/10.1016/j.surfcoat.2021.128077

The effect of temperature on water desorption and oxide formation in MoS_2 coatings and its impact on tribological properties

Kristine Dreva[a,*], Ardian Morina[a], Liuquan Yang[a], Anne Neville[a]

[a] *Institute of Functional Surfaces (iFS), School of Mechanical Engineering, University of Leeds, Leeds LS2 9JT, United Kingdom*

Abstract

Molybdenum disulfide (MoS_2) is used extensively in aerospace applications, where liquid lubricants are not suitable. MoS_2 has excellent tribological properties in vacuum, however, further research is required to fully understand the mechanisms taking place when exposed to varying temperatures in ambient atmosphere due to storage and on-ground testing. MoS_2 coatings were deposited on AISI 440C steel substrates, friction and wear tests were conducted at increasing temperatures, up to 75°C, determining the effect of temperature on wear mechanisms in air. It was found that the detected surface oxides do not impact tribological properties in MoS_2 at temperatures around 75°C. The water molecules at room temperature hinder the alignment of MoS_2 layers leaving some active edge sites exposed to contacting surfaces, leading to high friction and wear. Desorption of water molecules promote parallel alignment of layers, reducing shear strength, friction and wear.

Keywords: MoS_2 coating; Friction; Wear; Raman spectroscopy; Oxidation

*Corresponding author

Email address: pm16kdm@leeds.ac.uk (Kristine Dreva)

1. Introduction

MoS_2 has been used extensively in aerospace applications [1] due to its excellent tribological properties in vacuum and ultra-vacuum environments [2]. The effect of humidity on MoS_2 has been extensively researched, [3, 4] linking humidity and exposure to molecular oxygen, to formation of oxides such as molybdenum trioxide (MoO_3). MoS_2 coated mechanical systems can be stored in terrestrial environments for extended periods of time [5], leading up to 3.5% of MoS_2 to be oxidised, which can be much higher in porous MoS_2 coatings [4]. The formation of oxides due to humidity has been disputed, where Khare el.al [6] states that oxide formation is independent on oxygen exposure and the high friction in room temperature is only driven by the presence of water, where water molecules adsorb and diffuse through. Curry et al. [7] has observed that the extent of oxidation depends on the structure of MoS_2, where crystalline structure limits oxidation to the top 0.5 nm, in comparison to amorphous structure, where the oxidation depth can reach the bulk of the coating. Other studies [8], have suggested that water and oxygen, which are present during storage, causes the reaction (1) to occur:

$$2MoS_2 + 4H_2O + O_2 \rightarrow 2MoO_3 + 4H_2S \quad (1)$$

Contaminants such as oxygen and water molecules can be incorporated in MoS_2 during various stages, including deposition [9], storage [10] and operation, such as friction [6, 11]. During or after deposition process by physical vapour deposition (PVD), water vapour can be present in the chamber [9], leading to formation of $MoS_{2-x}O_x$ phase [12], with varying x value. This is caused by oxygen substitution, however, oxides do not form during deposition stage. $MoS_{2-x}O_x$ phase is not detrimental to tribological properties, as it has been reported

that substitutional oxygen helps to maintain low coefficient of friction (CoF) by facilitating intercrystalline slip [12]. From literature, it has been established that oxygen can interact with MoS_2 in two ways, it either substitutes suflur in a sulfur vacancy site, or it can form MoO_3, where O bonds with Mo [12], as per reaction (1). Recent studies [13] have also shown that partial oxidation leads to the formation of MoS_xO_y phase, where oxygen substitution is accompanied by edge site oxidation. Colas et.al [14, 15] has shown that the new phase formation is friction induced as the 3rd body film is composed of MoS_xO_y assisting easy shear between the contacting surfaces.

MoS_2 maintains low CoF at humidity levels below 5% relative humidity (RH) [8], above which significant reduction in coating lifetime has been observed. In another study, however, it was suggested that the humidity resistance is increased in Mo rich MoS_2, where the lifetime of the coating does not differ when exposed to the relative humidity of up to 20% [16].

However, on-ground testing of mechanical systems, such as solar arrays, can take place in ambient conditions, to ensure the integrity of the system before launch [17]. The coefficient of friction (CoF) of MoS_2 as a coating in ambient atmosphere ranges between 0.1-0.18 [6, 18]. Khare et al. [6] states that CoF increases with adsorbed water content, where water molecules are mostly physisorbed, which can be reversible with temperature increase, leading to reduced CoF.

Some conflicting studies exist when analysing the effect of high temperature on MoS_2 tribological properties. Meng et al. [19] states that excess oxide formation starts at temperatures between 300-350°C, where the rate of oxidation is higher than the oxide removal upon friction. On the contrary, it has been observed by Khare et al. [6] that excess oxide formation can start from 100°C and the accumulation of surface oxides starts to accelerate further at 200°C. Similar conclusion was provided by Serles et al. [20].

The effect of humidity on MoS_2 has also been well researched [21, 22, 6, 18, 23]. It has been established that CoF increases with the presence of humid air. In sputter deposited MoS_2, the increased CoF at temperatures below 100°C is not due to oxide formation. Instead, the increase is caused by physisorbed water molecules, leading to increased lamellar shear [9]. In the environments where high water content is present in the air, MoO_3 and H_2S are formed [8], degrading the tribological properties. Kubart et al. [24] suggested adhesion between interlayers takes place with water adsorption and diffusion through the structure, however, no chemical analysis was conducted to support this.

Overall, there is lack of chemical analysis that could help to explain the wear mechanism taking place at temperatures below 100°C, and as a result, some uncertainties exist in determining the effect of water molecule interaction with MoS_2. The majority of on-ground tests take place at room temperature (RT), which is approximately 25°C. Due to lack of chemical analysis in the literature, the failure mechanisms in air are unclear. Also the role of increasing temperature is unclear as it has always been assumed that temperature up to 100°C leads to desorbed water molecules, however, in-depth chemical analysis is lacking to confirm this.

In this study, Raman analysis was used to monitor structural changes in MoS_2 by analysing E^1_{2g} (in-plane) and A_{1g} (out-of plane) peak shifts. Testing temperatures ranging between 25°C - 75°C have been chosen to determine the presence and the role of oxides. This will allow to determine the failure mechanisms in ambient environment and the optimisation of operating conditions in air to maintain low friction and wear.

2. Methodology

2.1. Friction and wear

The experiments were conducted on dry contact reciprocating pin-on-plate tribometer equipped with a heating element located underneath the sample holder, as shown in Figure 1. The temperature of the sample was measured using a thermocouple connected to the sample holder. The materials used for the friction test is summarised in Table I, where the roughness was measured from three different locations for each sample.

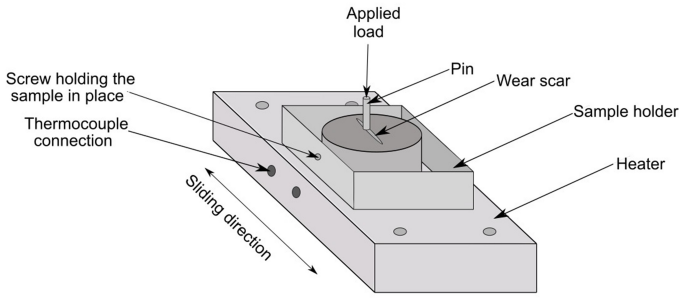

Figure 1: Reciprocating pin-on-plate tribometer set-up

Table I: Material properties

Body	**Material**	**Dimensions**	**Roughness (nm)**
Pin	EN31	40mm radius curvature	73.12 ±26.07
Plate	AISI 440C	30mm diameter, 6mm thick	20.57 ±0.76
MoS_2 coating	MoS_2	1μm thick	30.65 ±0.65

Each pin was sonicated in acetone for three minutes to remove impurities and debris, after which, isopropanol was used to rinse off the acetone and air gun was applied to dry the pin before installation. The coated plate was rinsed with heptane to remove any contamination without degrading the coating. The maximum contact pressure was 530 MPa, the sliding speed was set to 20 mm/s with 10 mm stroke length for 1800 cycles for all the tests, which

is equivalent of 30 minutes of testing. Friction tests were conducted in air at 25°C, 40°C and 75°C in ambient humidity. The laboratory air humidity was measured using a hygrometer and it was ranging between 35-50% RH. Each test was repeated at least three times to ensure repeatability. The average steady state CoF was calculated using the data points from 1200 - 1800 cycles (from 20-30 minutes of testing), for all the repeats. For every test, one CoF value was obtained per cycle, which is the average of forward and backward stroke for each cycle.

2.2. Coating

The MoS_2 coating was deposited by Teer Coatings Ltd (Droitwich, UK) using Physical Vapour Deposition (PVD), where DC closed-field unbalanced magnetron sputtering was used to deposit MoS_2 on AISI 440C steel substrates. After polishing, the substrates were sonicated in acetone for five minutes, followed by ethanol rinse and drying using an air gun. The substrates were stored in vacuum desiccator to avoid the formation of surface oxides.

Prior to deposition, the substrates were cleaned by sputtering Ti under argon atmosphere to remove any surface contaminants and to reduce water vapour. 100-200 nm of Ti was then deposited as an interlayer, followed by mixture of MoS_2 and Ti to further improve the adhesion of MoS_2, followed by pure MoS_2 coating with total thickness of 1 μm, using a recipe developed by Teer Coatings Ltd [25]. The deposition temperature is kept below 100°C with chamber base pressure of 5×10^{-5} mbar.

2.3. Characterisation

Raman spectroscopy was conducted in ambient conditions using a Renishaw InVia spectrometer (UK) with spectral resolution of 800 nm equipped with an Olympus objective lens. The argon ion laser at wavelength of 488 nm was focused using a 50× magnification objec-

tive lens, yielding laser diameter of 400 nm at laser power of 0.5 mW. Low laser power was selected to avoid laser induced oxidation of MoS_2. Raman maps were obtained by scanning an area of 24 $\times$ 20 μm^2 with laser step size of 2 μm. The exposure time for each scan was 8 s with two accumulations. Each map consisted of 13 $\times$ 11 Raman scans located in the middle of each wear scar, the edge of the wear scar and outside of the wear scar, which is an unworn area as illustrated in Figure 2. Each dot in Figure 2 represents a position of laser, where spectra is obtained. All the measurements within the wear scar (worn) were taken approximately 5 mm along the wear scar, which is the centre. The structure of the coating is analysed by obtaining the Raman peak shift of E^1_{2g} and A_{1g} modes, which are the in-plane (shear) and out-of-plane (stacking) vibrations respectively. Raman peak shift is used to determine structure distortion. This method is not used to determine number of layers as the coating contains over 6 layers and is considered as bulk. Raman was calibrated using Si crystal, ensuring the position of the Si peak remains 520 cm^{-1}. The average Si position was 520.0829 $\pm$ 0.254 cm^{-1}.

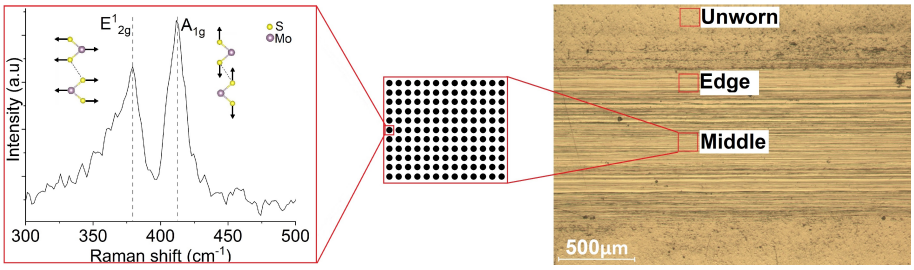

Figure 2: Raman mapping locations across the wear scar

The lattice structure of the coating and powder (molybdenum disulfide powder, Sigma Aldrich, US) was analysed using X-Ray Diffraction (XRD) PANalytical X'Pert PRO by Phillips, equipped with a secondary graphitic monochromator. The samples were scanned using nickel filtered Cu $K\alpha$ radiation ($\lambda = 1.54$ Å) with Bragg angle (2θ) ranging from 5-80°. The interlayer spacing was measured by analysing the (002) peak. The effect of temperature

increase on the coating structure was analysed by placing the sample in a hot stage, where temperature increase was set from 25°C to 200°C at rate of 2 °C/min. Each scan was taken at 10°C increments. The cooling rate was set to 10°C/min and the final scan was taken at 25°C. The crystallite size (D) along 002 plane, which is in c direction, was calculated using Debye-Scherrer equation [26] as per Equation 2:

$$D_{002} = \frac{k_{002} \times \lambda}{\beta_{002} \times cos\theta} \tag{2}$$

Where k=0.76 [27] and is the shape factor for MoS_2 particles. λ is the wavelength of X-Ray particles, θ is the diffraction angle and β is full width at half maximum (FWHM).

Wear analysis was conducted using NPFlex, non-contact white light interferometer by Bruker (USA) using vertical resolution of <0.15 nm. Three areas of each wear scar were scanned, ensuring repeatability. The data was analysed using Vison64 software and specific wear rate (W) was calculated using Archard's wear equation [28], as shown in Equation 3:

$$W = \frac{VL(mm^3)}{F(N) \times D(m)} \tag{3}$$

Where VL is the volume loss of the plate, F is the load applied and D is the sliding distance.

Surface morphology was analysed using scanning electron microscopy (SEM) by Carl Zeiss Evo MA15-SEM equipped with 80mm X-Max SDD detector. SEM is coupled with energy dispersive X-ray spectroscopy(EDX) with AZtecEnergy EDX system and CZ STEM detector, used for elemental analysis. Accelerating voltage of 20kV was used for elemental analysis and 5kV was used to improve the deconvolution of Mo and S peaks.

3. Results

3.1. Wear scar analysis

The average steady state CoF at RT is 0.17. When test temperature is increased to 40°C, the average CoF is 0.06 and it drops further to 0.04 when the test temperature is increased to 75°C, which is in an agreement with literature [18, 20]. Clear distinction between friction behaviour at small temperature increase is observed in Figure 3(a). It has been suggested that increased temperature reduces friction due to desorbed water molecules [18], restoring the low interfacial shear. The wear rate is in agreement with the friction curves, where the wear rate is lowest at 75°C and highest at 25°C as shown in Figure 3(b).

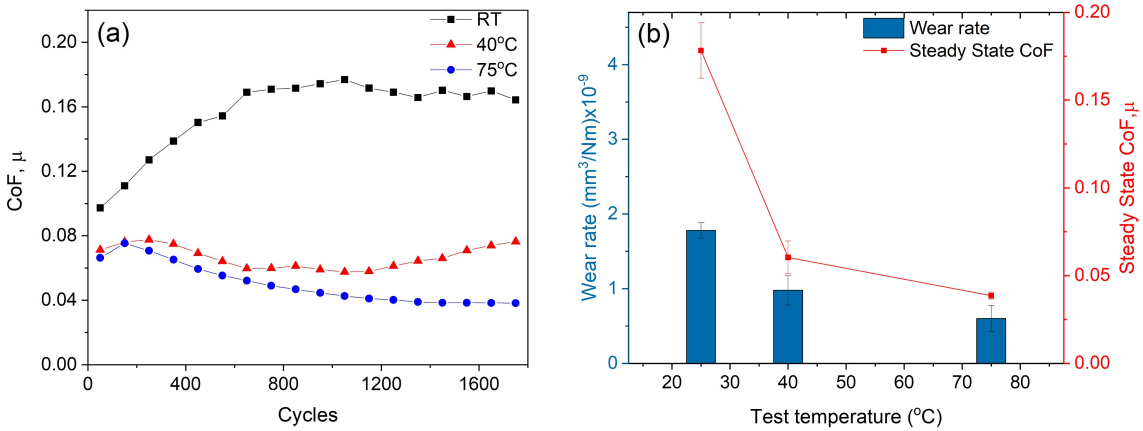

Figure 3: (a) Friction coefficient curves in MoS_2 coating at 25°C (RT), 40°C and 75°C, (b) average steady state CoF and specific wear rate of MoS_2 at increasing test temperatures

Wear scar profiles in Figure 4 show the wear depth at RT (Figure 4(a)) and at 75°C (Figure 4(b)), where the grey area show the thickness of the coating. At RT, wear depth increases with cycles without build-up of loose debris and therefore, very minimal amounts or no tribofilm is formed. In this study, a tribofilm is referred to as an altered layer of MoS_2 which forms during friction and wear. This layer consists of debris that is trapped between contacting surfaces as well as transfer film that has been re-adhered to the wear scar from

the counterbody. The formation of this film is dependant on various parameters, such as the contact pressure applied, environment and contaminants present.

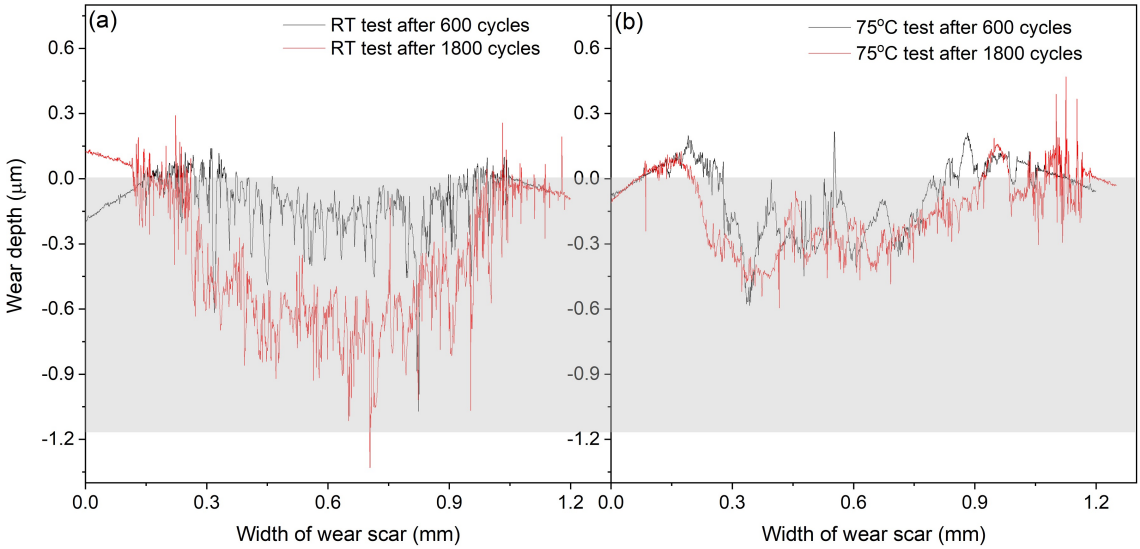

Figure 4: (a) Wear scar profiles of RT test after 600 cycles (black) and 1800 cycles (red) and (b) 75°C wear scar profiles after 600 cycles (black) and 1800 cycles (red), the grey area illustrates the thickness of the coating

White light interferometer images of the wear tracks are illustrated in Figure 5. It is clear that at RT, very little debris remains within the wear scar and significant material loss in seen after 1800 cycles (c). At increased temperature, wear particles are re-distributed across the wear scar due to agglomeration (d). These particles then contribute to the formation of tribofilm.

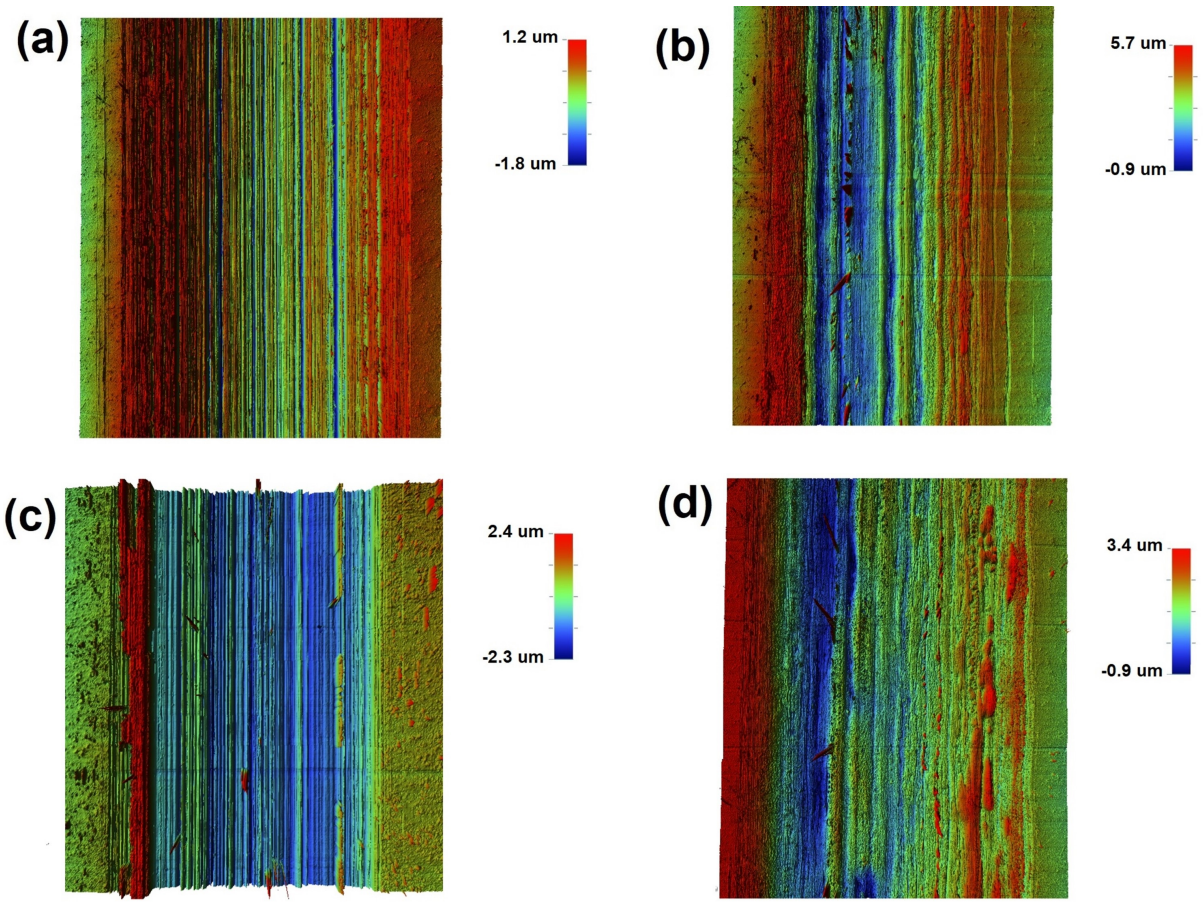

Figure 5: 3D wear scar profiles of wear scars after 600 cycles generated at (a) RT and (b) 75°C, and after 1800 cycles generated at (c) RT and (d) 75°C

When test temperature is increased to 75°C, after 600 cycles, the roughness of the wear scar decreases with increasing cycles. This is shown in Figure 6(b), indicating that the valleys created during run-in stage are being sealed, forming a tribofilm, therefore, yielding low shear between MoS_2 and the counterface. This is also seen in wear rate measurements at 600 cycle increments (Figure 6(a)), where the wear rate decreases due to efficient tribofilm formation.

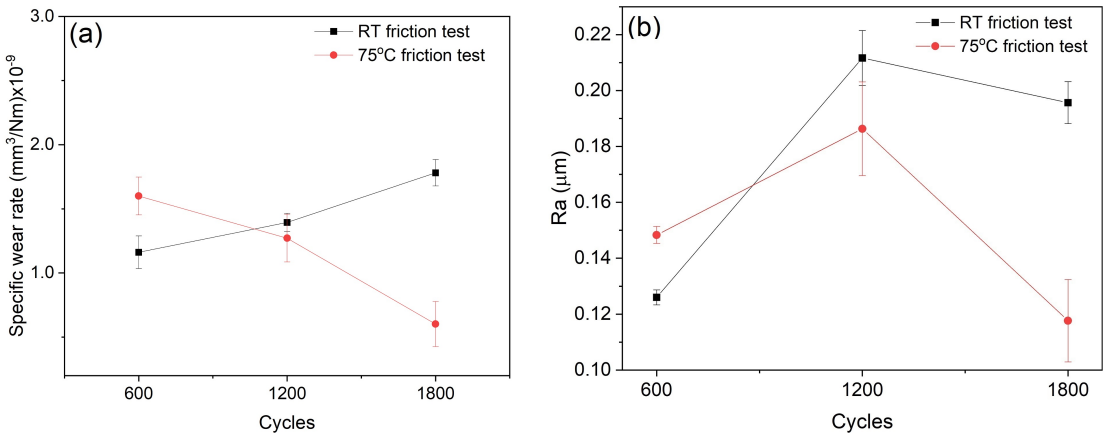

Figure 6: (a) Specific wear rate of MoS_2 coated plate and (b) wear scar roughness measurements after 600 cycle increments for tests conducted at RT and 75°C

It has been suggested by Colas et al. [29] that at RT, large 3rd body particles are formed, which are too large to get trapped between the contacting surfaces. Instead of forming a tribolayer, these particles migrate outside of the wear scar, leading to material loss. This has been observed in RT wear scar profile, where valleys are seen, whereas at increased temperature, the valleys are refilled, forming tribofilm. This supports the 3rd body wear hypothesis [29, 30], where large particles lead to increased wear and small particles agglomerate together, without being ejected out of the wear scar. Large debris particles are seen in RT generated wear scar in Figure 7(a) and very small particles are seen at 75°C in Figure 7(b). The difference between worn MoS_2 at RT (c) and at 75°C (d) shows that at increased temperature, the re-distributed debris forms a 3rd body film. This supports the white light interferometry images of particle re-distributiuon and agglomoration.

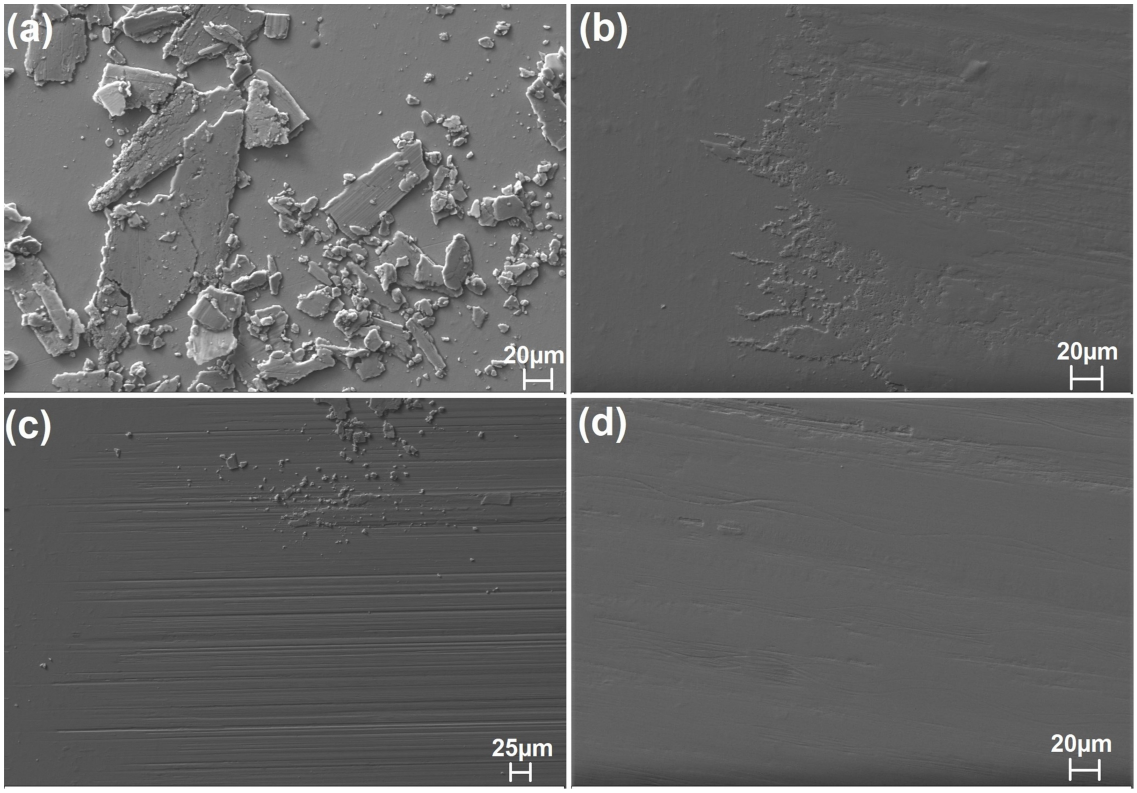

Figure 7: SEM image of (a) debris at RT, (b) wear scar tip at 75°C, (c) wear scar tip at RT and (d) wear scar at 75°C

The crystallite size of MoS_2, which was obtained by using Debye-Scherrer equation, does not change significantly at RT as shown in Figure 8. With exposure to increased temperature, in unworn MoS_2, small increase in crystallite size is seen, however, after 600 cycles at 75°C, the crystallite size decreases, indicating reduction in long range order. Also no significant layer re-orientation takes place at RT.

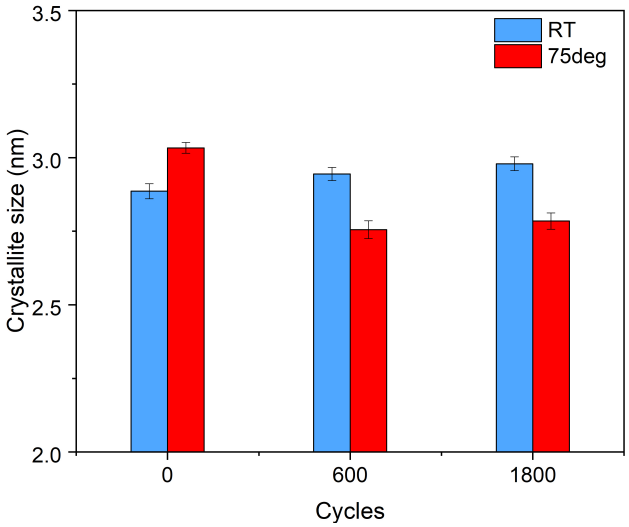

Figure 8: Crystallite size of unworn (at 0 cycles) and worn coating after 600 and 1800 cycles at RT and 75°C

Raman analysis of each wear scar on the coated plate provides the analysis of the E^1_{2g} and A_{1g} peak shift which are shown in Figure 9 (a). Only the mean peak position is plotted, which is obtained by taking the mean and standard deviation of all the scans per Raman map. This ensures that the peak shifts are statistically significant.

The peak positions were compared between worn and unworn coated plate, shown in Figure 9. The average peak shifts of unworn MoS_2 were analysed to determine the chemical changes that are only induced by heat. The standard deviation of unworn peak shifts is shown within the shaded area for each peak.

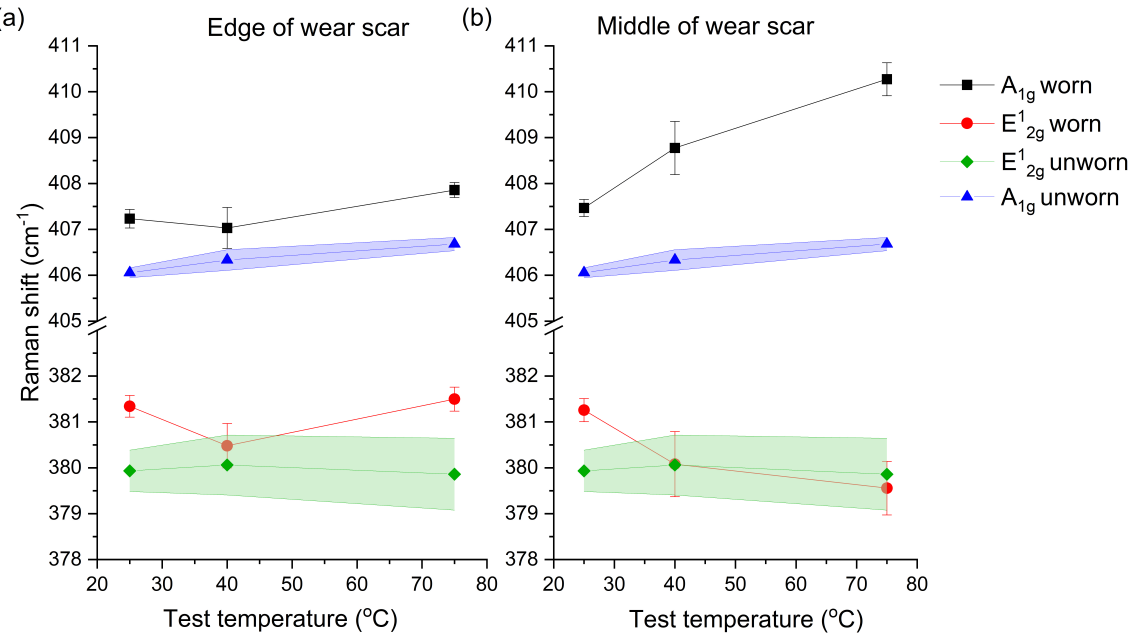

Figure 9: E^1_{2g} and A_{1g} Raman peak position shifts with increasing temperature, the shaded area is standard deviation at increasing temperature, with analysis conducted on (a)the edge and (b)the middle of the wear scar

Raman analysis has been conducted on the edge and the middle of the wear scar, as shown in Figure 2. At the edge of the wear scar, A_{1g} and E^1_{2g} peaks shifted upwards. Distinct differences in peak shifts are seen in the middle of the wear scar (Figure 9(b)) at increased temperatures. At RT, both peaks have shifted by 1.3cm^{-1}cm. At 40°C both peaks start to shift at different increments, with the largest shift difference seen at 75°C, where A_{1g} has increased by 3.6cm^{-1} and E^1_{2g} peak has decreased by 0.30cm^{-1}, in comparison to unworn coating at 40°C and 75°C. The peak shift, where A_{1g} and E^1_{2g} mode increased and decreased, respectively, is consistent with defect formation. The most favourable defect is loss of sulfur [31], which can be detected by Raman as both A_{1g} and E^1_{2g} vibrational modes rely on the vibration of S atoms.

A_{1g} and E^1_{2g} peaks of unworn coating and tribofilm (Figure10(a)) located at the tip of the wear scar show a clear shift between test temperatures. The structure of the tribofilm was analysed by comparing the distance between A_{1g} and E^1_{2g} Raman peaks. Average peak

distance is shown in Figure 10(b), where the error bars show standard deviation of all the scans per Raman map. Only a small amount of Raman scans were taken from a tribofilm to ensure all the scans are focused, as the tribofilm at the end of the scar is rigid and uneven. The RT generated tribofilm does not differ significantly from untested coating, as it was already confirmed that only small amount or no tribofilm was formed at RT. The structure of a tribofilm generated at 75°C matches the structure in the middle of the wear scar, as shown in Figure 9(b). This confirms that tribofilm is present across the wear scar at increased temperature.

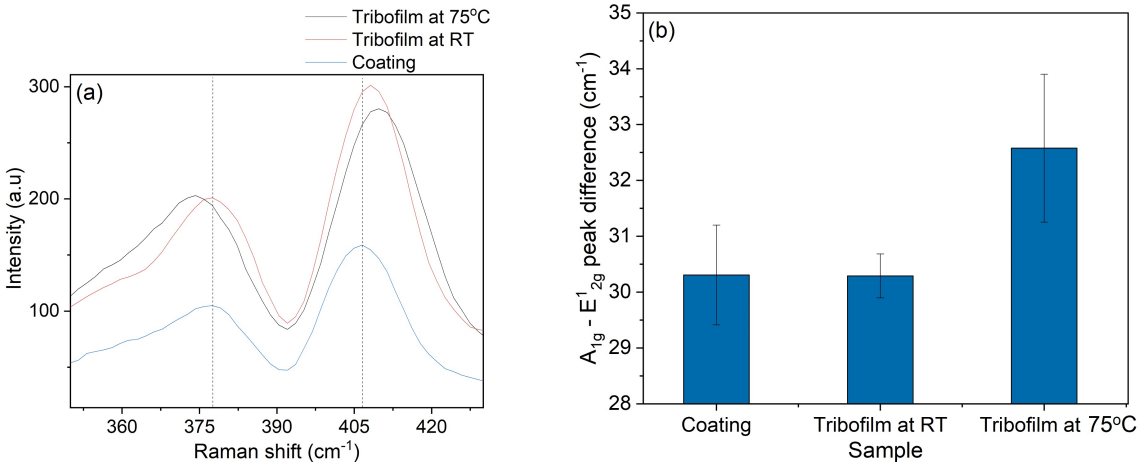

Figure 10: (a) Raman peak shift of E^1_{2g} and A_{1g} modes of coating and tribofilms, generated at RT and 75°C, (b) average E^1_{2g} and A_{1g} peak separation distance

Full width at half maximum (FWHM) of A_{1g} mode is shown in Figure 11, as A_{1g} peaks are more defined. FWHM with standard deviation of unworn coating for each temperature is shown within the shaded area. Significant FWHM difference is seen between coating and powder MoS_2, where the untested coating has FWHM of 7.93cm^{-1} and in powder MoS_2 it is 3.51cm^{-1}.

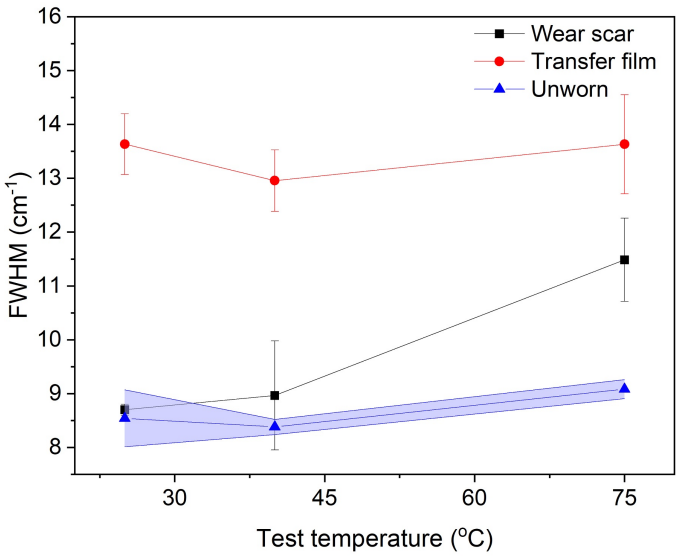

Figure 11: FWHM of A_{1g} mode in the middle of the wear scar and the transfer film on the counter body. The shaded area is the standard deviation of FWHM, taken outside the wear scar at increasing test temperature

This difference is due to impurity incorporation into the structure of the coating during deposition process [32], leading to reduced crystallinity of MoS_2. This has also been confirmed by XRD, where significant peak shift is seen in coating, indicating the distance between the layers is increased and the crystallinity is decreased. The largest increase in FWHM is seen in the middle of the wear scar at increased temperatures. 2.40cm^{-1} increase is seen at 75°C in the middle of the wear scar, in comparison to the unworn area outside the wear scar. The transfer film on the counter surface is more distorted than the coating and therefore, no significant changes between temperatures in the transfer film is seen.

To gain further understanding of the structural changes of MoS_2, the difference in layer interspace distance of the coating in (002) plane was analysed using XRD with increasing temperature. Some tensile stress is present in the coating as the layer distance increases from 6.15$\mathring{A}$ in powder MoS_2 to 6.46$\mathring{A}$ in MoS_2 as a coating. It has been previously suggested that MoS_2 forms tensile stress due to incorporation of impurities during deposition [33], which can lead to crack growth. It has also been confirmed that the strain is not reduced with

increasing temperatures, where Figure 12(a) shows whether the interlayer distance changes when temperature is increased to 200°C. The error bars indicate the standard deviation of three separate test runs. No significant changes in the interspace are observed, confirming that the reduction in friction and wear at increased temperature is not due to decrease in strain, which has been introduced during deposition stage. The distance between the S-Mo-S layers can also be increased by exposure to water molecules, as shown in Figure 12(b).

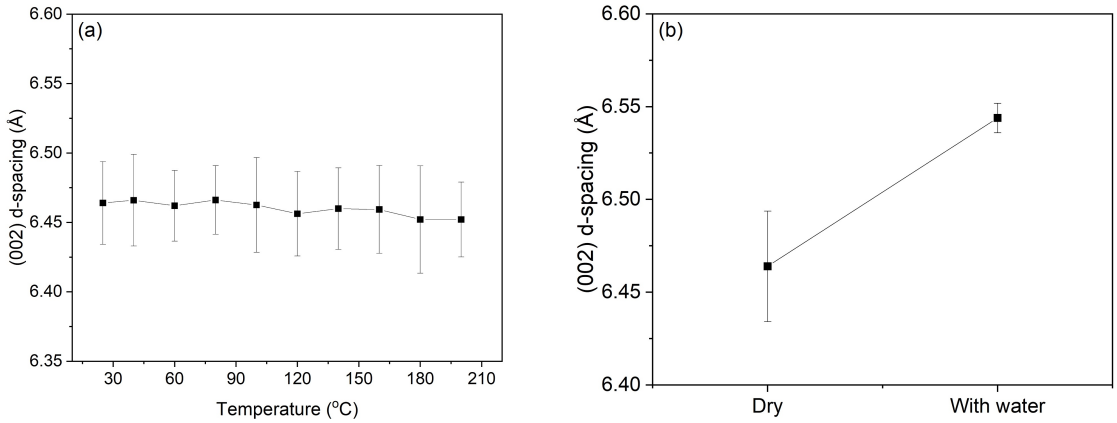

Figure 12: Interlayer spacing evolution of (002) plane in MoS_2 coating with (a) temperature increase from 25°C to 200°C and (b) before and after exposure to water

It is clear that water alone does not induce oxidation, as shown in Figure 13, where Raman spectrocsopy analysis was used to map the distribution of molybdenum oxides on unworn coatings, therefore the increase in layer distance is not formed due to the presence of oxides. It has also been shown that water molecules do not favour intercalation between the layers [34]. It is, however, possible that the layer distance increase is due to the formation of $MoS_{2-x}O_x$ phase [35]. In the case of O substitution, the layer distance increases as the distance between S-S decreases, forming compressive strain in the direction perpendicular to the layers and as a result, tensile strain is formed between the layers.

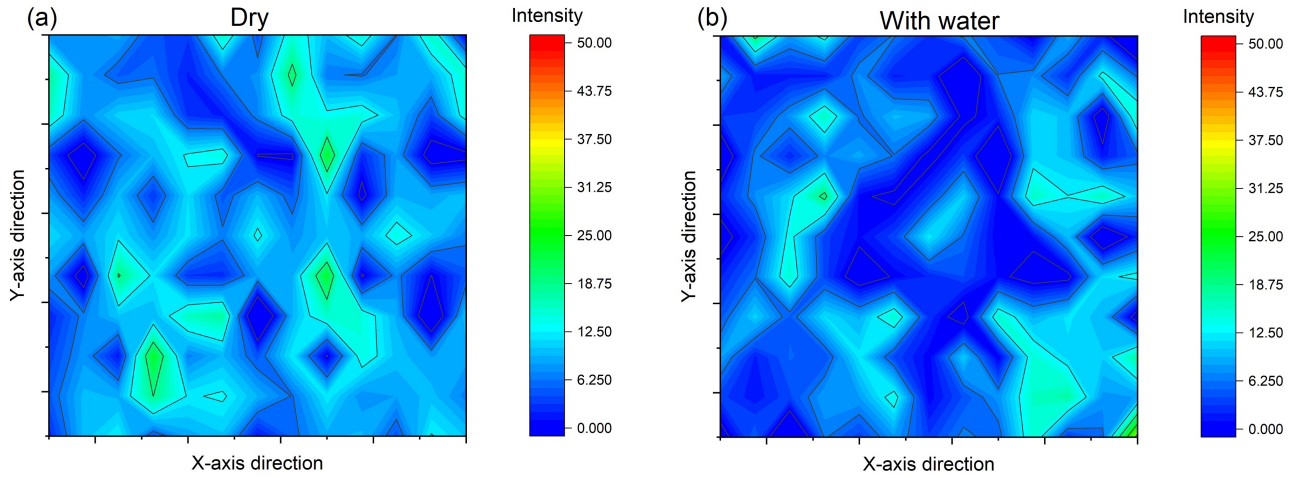

Figure 13: Raman map of 820 cm^{-1} peak intensity, mapping oxide distribution in (a) dry MoS_2 and (b) after the addition of water to the surface of unworn MoS_2

The migration of elements during friction test at various temperatures is shown in Figure 14, obtained by EDX, where large amounts of Fe is observed in RT friction tests and least amount at elevated temperatures, which is due to efficient tribofilm formation. Slight increase in oxygen is observed at 75°C, however this increase has not hindered the reduction of CoF and wear. Ti was also monitored in worn coatings, as Ti is used as an interlayer. It is clear that Ti does not increase with wear and therefore is not significantly exposed after wear.

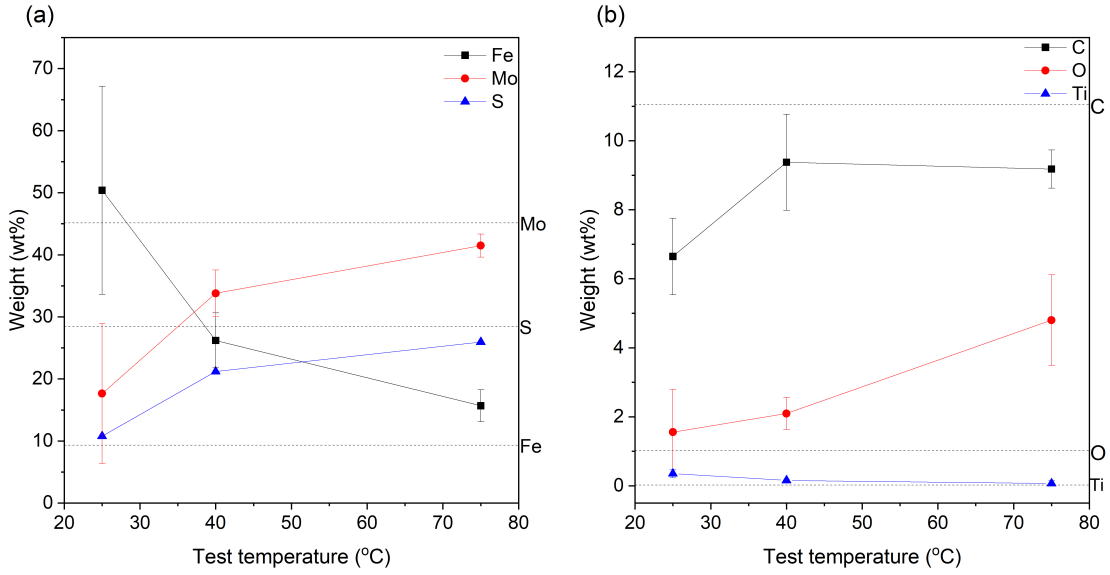

Figure 14: EDX elemental analysis of MoS_2 wear scar

EDX was also used to obtain the atomic weight % ratio between S and Mo, as shown in Figure 15, where the ratio of 2 indicate defect free structure. It is clear that the ratio has been reduced after high temperature wear, confirming loss of sulfur, as suggested by Raman analysis. As the analysis of S and Mo is semi-quantitative by EDX, the ratio was compared between accelerating voltage of 20 and 5kV, as suggested by Ehni and Singer [36].

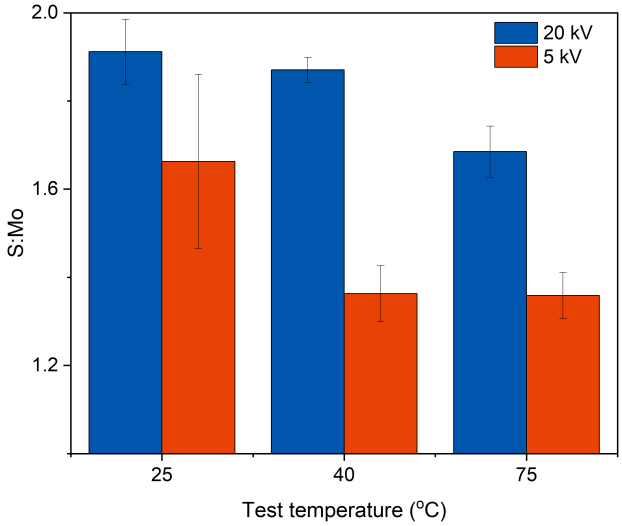

Figure 15: The ratio between S and Mo in worn MoS_2 using EDX, where the ratio of 2 indicates no loss of S

3.2. Transfer film analysis

The low CoF is achieved due to the efficient transfer film formation, which is observed on the pins in Figure 16, showing the optical microscope image of each pin in 600 cycle increments. MoS_2 is present on all pins, however, the distribution of MoS_2 varies with temperature. At 75°C, instead of forming a uniform film throughout the contact area, it appears that the transfer film forms through accumulation of loose debris first, which then is distributed throughout the contact area. Very small amounts of MoS_2 are found in the middle of the counter body wear scar after 600 cycles, where weak MoS_2 Raman signals are detected (Figure 16(d)), in comparison to uniform coverage after 1800 cycles (Figure 16(f)).

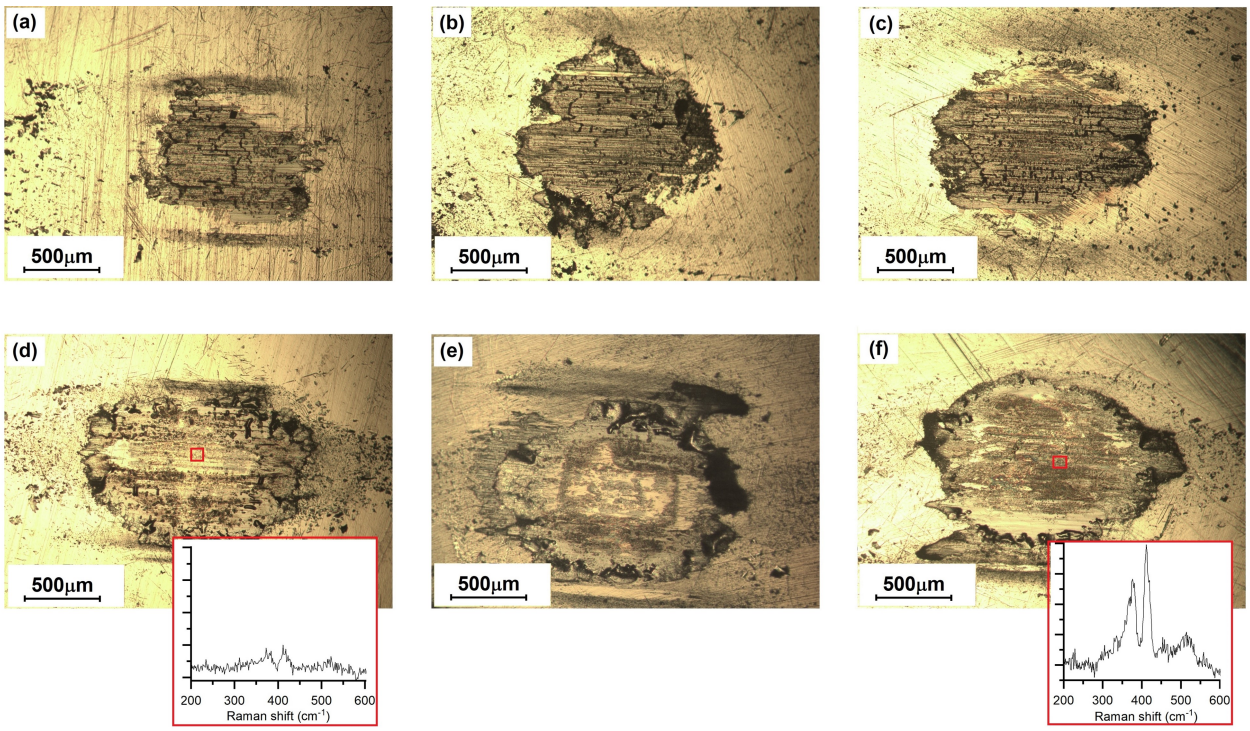

Figure 16: Optical microscope image of the counterbody and Raman analysis of the transfer film or debris at RT after (a) 600 cycles, (b) 1200 cycles, (c) 1800 cycles and transfer films generated at 75°C after (d) 600 cycles, (e) 1200 cycles and (f) 1800 cycles

After a uniform transfer film is formed, valleys in the wear scar are sealed, maintaining low friction and wear. This has been confirmed in Figure 6, where the wear starts to reduce after 1200 cycles at 75°C, which is when the accumulated debris is distributed. To confirm the distribution of MoS_2, normalised intensity of A_{1g} peak is mapped in Figure 17. The transfer film at 75°C show a significant intensity increase after run-in in Figure 17(d).

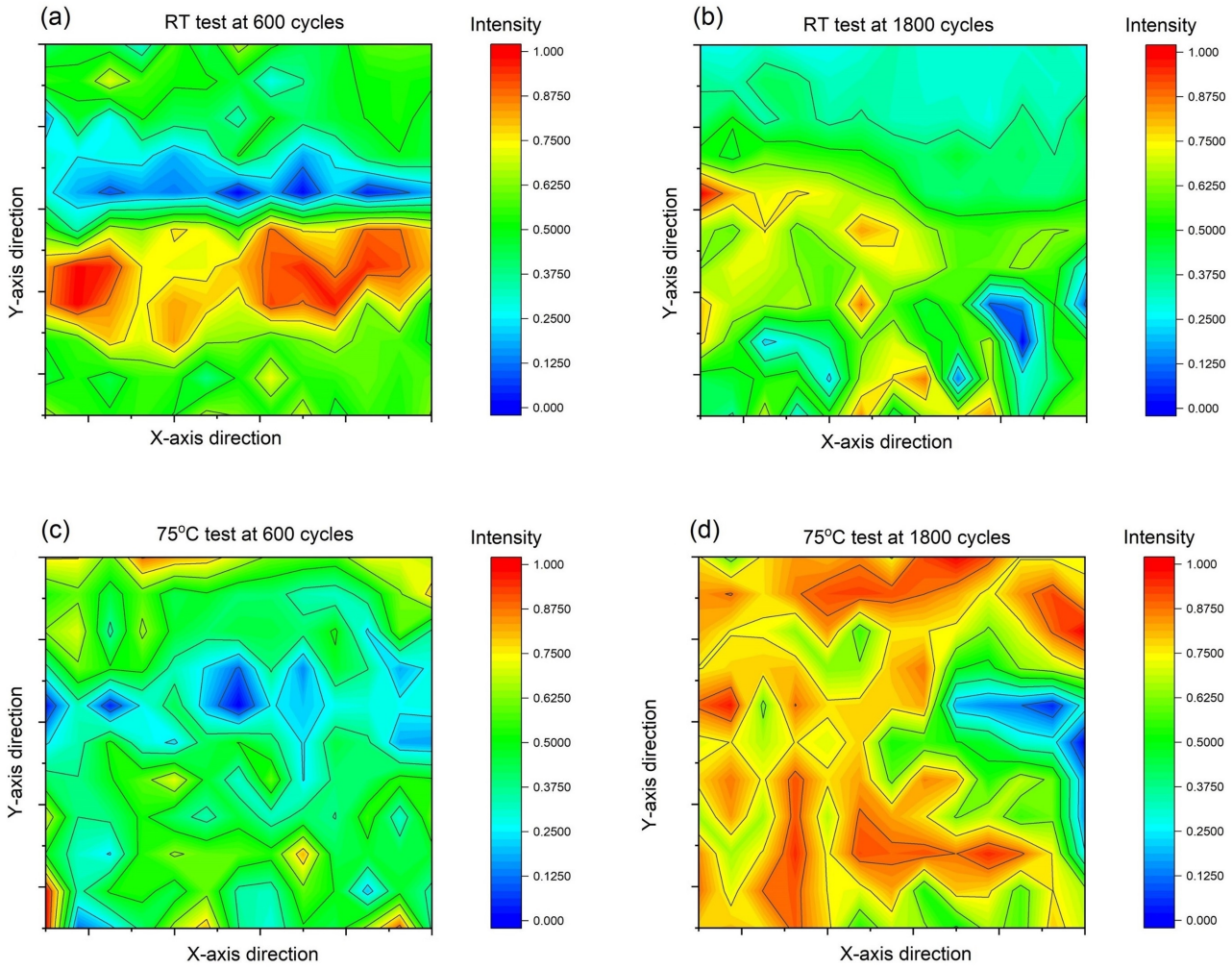

Figure 17: Raman maps of RT (a,b) and 75°C (c,d) transfer films, visualising the normalised intensity of A_{1g} peak

The presence of MoO_3 in transfer film is visualised in Figure 18 by mapping the intensity of dominant Raman peak for MoO_3 at around 820cm^{-1}, where very minimal amounts of oxides are present in RT transfer film after 600 cycles (a) and after 1800 cycles (b). However, at increased temperature, significant increase in oxide formation is observed, only after run-in and steady state. The increase in oxygen is also supported by EDX analysis.

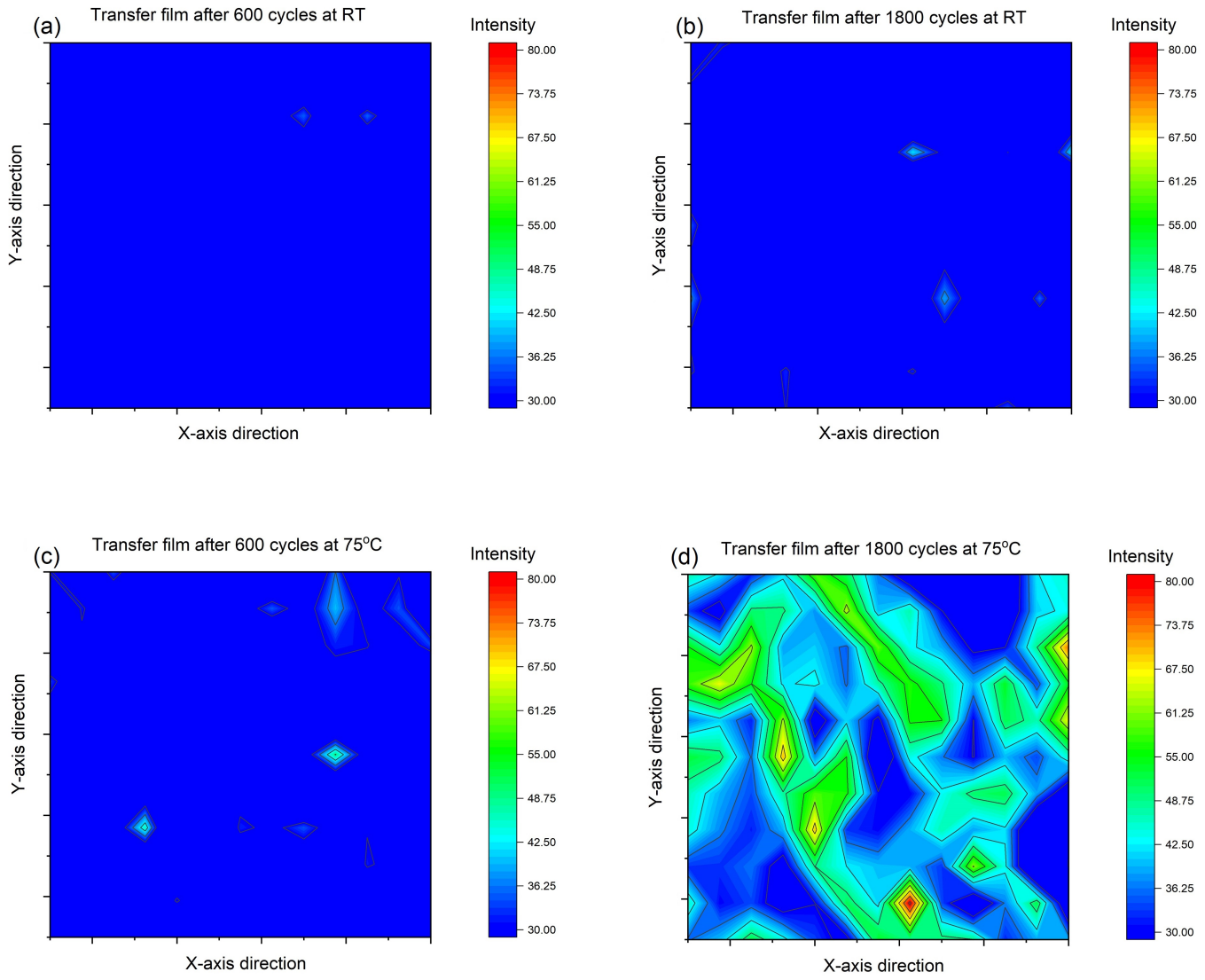

Figure 18: Raman maps consisting of 820cm^{-1} peak intensity visualising the presence of MoO_3 in transfer film at RT after (a) 600 cycles and (b) 1800 cycles, and transfer film at 75°C after (c) 600 cycles and (d) 1800 cycles

The structure of the pin transfer film is analysed by examining Raman peak shift. The mean distribution of each peak is shown in Figure 19. Increase of 4.6cm^{-1} in A_{1g} mode and decrease of 2.1cm^{-1} in E^1_{2g} mode at 75°C is seen. The large peak separation is due to breakage of Mo-S bonds, leading to loss of S and formation of defects in the structure [37, 38, 31].

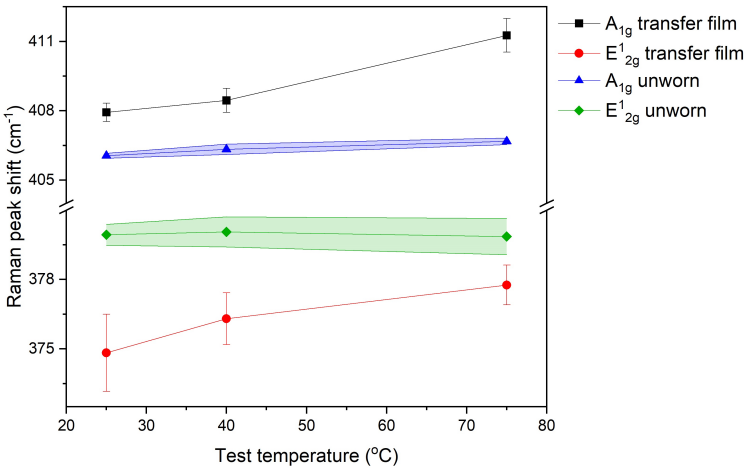

Figure 19: Raman analysis of the pin wear scar with peak difference between untested MoS_2 coating and the pin taken from the middle of the pin, with shaded areas representing standard deviation of unworn peak positions at increasing test temperatures

4. Discussion

It is clear that the structure distortion of MoS_2 begins with deposition process, where impurities, such as oxygen, are incorporated within the structure, leading to increased distance between layers, which was confirmed by XRD. It has been suggested that oxygen can be incorporated between the layers during deposition, which increases the layer distance of MoS_2 [39], leading to tensile stress formation. This can also lead to crack growth where the shear between the layers is disturbed due to misalignment and S-S interlocking [40]. Wahl et al. [41] has also proposed that the large interlayer distance is due to some defect formation.

During sliding, the top layer is deformed, where wear depth can reach up to $1\mu m$ at RT, which is almost the entire thickness of the coating. This is in agreement with EDX analysis, where Fe increases significantly within RT wear, indicating some substrate and interlayer exposure. Despite the large increase in Fe after RT wear, only minimal amount of Ti was detected, with negligible Ti increase at RT in comparison to increased temperature wear. It is possible that Ti is removed with wear, without affecting tribological properties of the film.

The CoF increases during run-in stage, and maintains the increase in the steady state. The unstable CoF generates deformed 3rd body particles which are brittle [29] and are ejected out of the wear scar, forming valleys which are not sealed. It has been suggested by Martin [42] that upon sliding, lattice rotation takes place, causing mismatch between the lattices, leading to a pile-up of superimposed crystallites. Therefore, a build up of transfer film is seen on the pin. However, despite the formation of transfer film, lack of tribofilm was observed at RT due to material loss. Tribofilm was detected at 75°C by Raman, where E^1_{2g} peak starts to downshift and A_{1g} peak up-shifts. This has not been observed on the outside and the edge of the wear scar and is in agreement with structural defects [31] being introduced during heating and wear. The presence of defects within the wear scars was also supported by EDX, where S:Mo ratio was obtained. Despite the increased density of defects, the CoF and wear remain low at 75°C. Defects aid the re-orientation of planes, leading to formation of dense films. At increased temperature, less energy is required to break S-Mo-S bonds [43], leading to more loose debris being generated in comparison to RT generated wear. The source of defects in the wear scar originates from transfer film re-distribution, forming dense amorphous film. It has been suggested that low shear at increased temperature is due to thermal expansion of interlayers [20], however, XRD results (Figure 12(a)) show that thermal expansion does not take place at temperatures up to 200°C. Therefore, thermal effects on their own do not contribute to weakening of Van der Waals forces between the layers.

It has been suggested that the increase in crystallinity is shear induced [44]. However, the XRD measurements of untested MoS_2 at RT and MoS_2 that has been exposed to 75°C, illustrate some increase in crystallinity at 75°C, due to the appearance of (100) plane, which is absent in RT coating, as shown in Figure 20(a). The broad (002) peak indicates lack of crystallinity, which can be compared to a crystalline MoS_2 powder structure, where a

sharp peak is shown in Figure 20(b). The emerging (100) peak in Figure 20(a) indicates increased order, where more than one orientation can be detected [45]. This crystallinity is then reduced after wear at 75°C, where (002) peak has reduced in intensity and (100) peak is less distinct. This is also supported Raman spectroscopy (Figure 11). At RT, a mixture of parallel and perpendicular orientated layers are present.

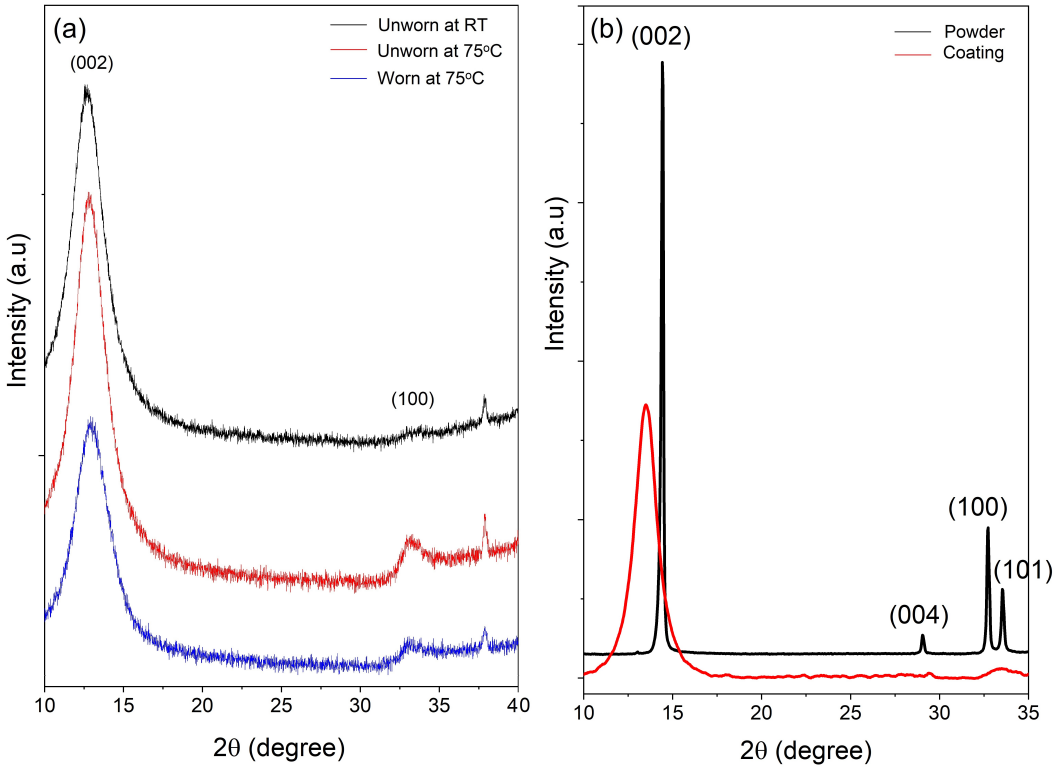

Figure 20: (a) XRD of unworn MoS_2 coating at RT, 75°C and worn coating at 75°C, (b) XRD of MoS_2 as a coating and crystalline powder

The layers that are perpendicular to the substrate have active edge sites exposed to the uncoated steel surface [46], leading to high adhesion between MoS_2 and the steel pin. The reorientation of lattice planes at increased temperature is possibly due to water desorption, leading to realignment of layers. Water desorption at increased temperatures is supported in previous studies [6, 20]. Furthermore, it was observed in this study, that the exposure of MoS_2 to high temperatures in air leads to oxygen substitution, which can have atomically 'smoothing' effect [12]. Therefore, it has been assumed that water desorption can lead to

layer re-orientation. On contrary, without the increase in temperature, the physisorbed water molecules, form H bonds with sulfur [47], leading to lack of layer re-orientation upon friction.

Very small amounts of oxides were detected in RT wear scar, which were confirmed by Raman and EDX, therefore the oxygen content in the coating is not responsible for high friction and wear. Similarly, oxides were found in transfer film at increased temperature but reduction in friction and wear were seen, confirming that the surface oxides which do not get removed during friction, do not affect tribological properties of the coating. This is in agreement with Serles et.al [20] and Khare et.al [6], where the friction and wear is not dependent on oxide formation below 100°C as the surface oxides get removed. However, in-depth Raman spectroscopy in this study shows defect formation, which leads to oxygen substitution and oxide formation at 75°C, which is not removed with wear. It was also shown in Figure 9, that increased temperature on its own induces very minimal changes, where some strain can be induced, however this is negligible. The lack of detected structural changes support oxygen substitution, which has restored the structure. Upon friction, further substitution leads to excess oxide formation. Due to the strong oxygen bonding energy [48], the excess oxides in the transfer film improve the adhesion of the transfer film and due to the debris re-entry and formation of tribofilm, no significant abrasive wear was observed, in comparison to RT wear.

5. Conclusion

Tribological properties of MoS_2 coatings have been determined in air to gain full understanding of the optimal conditions that contribute to low friction and wear. Test temperature ranged from RT to 75°C in order to analyse formation of oxides and its influence on shear strength.

- At RT, surface oxides are removed during friction due to large debris formation and material loss. However, the removal of oxides does not reduce the shear between the layers. In contrast, at 75°C these oxides are not removed. This is due to the formation of small particles that are re-introduced between the contacting surfaces, forming a tribofilm that contributes to low shear.

- Transfer film structure on the pin consists of defects, as shown by Raman analysis. This is due to Mo-S bond breakage during shear. At 75°C, this film is re-deposited on the wear scar and therefore, defects are detected on both surfaces. Due to these defects, the adhesion of transfer film to the counter-body is improved.

- At RT, some layers are orientated perpendicular to the substrate, exposing active edge sites to steel surface leading to high adhesion of particles. This is avoided at 75°C, where layers are orientated parallel to the substrate.

- During friction at 75°C, small wear particles are formed that agglomerate together and they are small enough to remain between the contacting surfaces. The agglomeration can be observed in transfer film formation where a build up of debris starts around the contacting area and gets distributed across, during steady-state.

Overall, it can be concluded that the excess surface oxides in MoS_2 are generated in small quantities, and therefore it does not impact tribological properties at temperatures around 75°C. Desorption of water molecules can lead to re-orientation of MoS_2 layers, restoring low shear strength and improving the formation of transfer film. At RT, these contaminants are present in the structure, leading to exposure of active edge sites that adhere to the counter surface causing high friction and wear as well as material loss. Therefore, small temperature increase can be beneficial to the tribological properties of MoS_2 in air.

Acknowledgements: Thanks to Adam Wade and Joshua Armitage from University of Leeds, for providing assistance in Raman map analysis development. Also thanks to Teer Coatings Ltd for providing MoS_2 coatings. This work was funded by EPSRC (Engineering and Physical Sciences Research Council) grant number EP/L01629X/1.

References

[1] X. Gao, M. Hu, J. Sun, Y. Fu, J. Yang, W. Liu, L. Weng, Changes in the composition, structure and friction property of sputtered mos2 films by leo environment exposure, Applied surface science 330 (2015) 30–38.

[2] X. Gao, M. Hu, J. Sun, Y. Fu, J. Yang, W. Liu, L. Weng, Response of rf-sputtered mos2 composite films to leo space environment, Vacuum 144 (2017) 72–79.

[3] Z. Chen, X. He, C. Xiao, S. H. Kim, Effect of humidity on friction and wear—a critical review, Lubricants 6 (3) (2018) 74.

[4] J. R. Lince, S. H. Loewenthal, C. S. Clark, Tribological and chemical effects of long term humid air exposure on sputter-deposited nanocomposite mos2 coatings, Wear 432 (2019) 202935.

[5] E. Roberts, Space tribology: its role in spacecraft mechanisms, Journal of Physics D: Applied Physics 45 (50) (2012) 503001.

[6] H. Khare, D. Burris, Surface and subsurface contributions of oxidation and moisture to room temperature friction of molybdenum disulfide, Tribology Letters 53 (1) (2014) 329–336.

[7] J. F. Curry, M. A. Wilson, H. S. Luftman, N. C. Strandwitz, N. Argibay, M. Chandross, M. A. Sidebottom, B. A. Krick, Impact of microstructure on mos2 oxidation and friction, ACS applied materials & interfaces 9 (33) (2017) 28019–28026.

[8] M. Buttery, S. Lewis, A. Kent, R. Bingley, M. Cropper, Long-term storage considerations for spacecraft lubricants, Lubricants 8 (3) (2020) 32.

[9] J. R. Lince, Effective application of solid lubricants in spacecraft mechanisms, Lubricants 8 (7) (2020) 74.

[10] M. R. Vazirisereshk, A. Martini, D. A. Strubbe, M. Z. Baykara, Solid lubrication with mos2: a review, Lubricants 7 (7) (2019) 57.

[11] C. Muratore, J. E. Bultman, S. M. Aouadi, A. A. Voevodin, In situ raman spectroscopy for examination of high temperature tribological processes, Wear 270 (3-4) (2011) 140–145.

[12] P. D. Fleischauer, J. R. Lince, A comparison of oxidation and oxygen substitution in mos2 solid film lubricants, Tribology international 32 (11) (1999) 627–636.

[13] Z. Zheng, S. Cong, W. Gong, J. Xuan, G. Li, W. Lu, F. Geng, Z. Zhao, Semiconductor sers enhancement enabled by oxygen incorporation, Nature communications 8 (1) (2017) 1–10.

[14] G. Colas, A. Saulot, D. Philippon, Y. Berthier, D. Léonard, Time-of-flight secondary ion mass spectroscopy investigation of the chemical rearrangement undergone by mos2 under tribological conditions, Thin Solid Films 588 (2015) 67–77.

[15] G. Colas, S. Pajovic, A. Saulot, M. Renouf, P. Cameron, A. Beaton, A. Gibson, T. Filleter, Adhesion measurements in mos2 dry lubricated contacts to inform predictive tribological numerical models: comparison between laboratory-tested samples and ball bearings from the niriss mechanism, in: ESMATS 2017, 2017.

[16] K. Matsumoto, M. Suzuki, Tribological performance of sputtered mos˜ 2 films in various environment-influence of oxygen concentration, water vapor and gas species, EUROPEAN SPACE AGENCY-PUBLICATIONS-ESA SP 438 (1999) 43–48.

[17] H. W. Brandhorst Jr, J. A. Rodiek, Space solar array reliability: a study and recommendations, Acta Astronautica 63 (11-12) (2008) 1233–1238.

[18] E. Serpini, A. Rota, A. Ballestrazzi, D. Marchetto, E. Gualtieri, S. Valeri, The role of humidity and oxygen on mos2 thin films deposited by rf pvd magnetron sputtering, Surface and Coatings Technology 319 (2017) 345–352.

[19] F. Meng, C. Yang, H. Han, Study on tribological performances of mos2 coating at high temperature, Proceedings of the Institution of Mechanical Engineers, Part J: Journal of Engineering Tribology 232 (8) (2018) 964–973.

[20] P. Serles, K. Gaber, S. Pajovic, G. Colas, T. Filleter, High temperature microtribological studies of mos2 lubrication for low earth orbit, Lubricants 8 (4) (2020) 49.

[21] J. F. Curry, N. Argibay, T. Babuska, B. Nation, A. Martini, N. C. Strandwitz, M. T. Dugger, B. A. Krick, Highly oriented mos 2 coatings: tribology and environmental stability, Tribology Letters 64 (1) (2016) 11.

[22] A. Schumacher, N. Kruse, R. Prins, E. Meyer, R. Lüthi, L. Howald, H.-J. Güntherodt, L. Scandella, Influence of humidity on friction measurements of supported mos2 single layers, Journal of Vacuum Science & Technology B: Microelectronics and Nanometer Structures Processing, Measurement, and Phenomena 14 (2) (1996) 1264–1267.

[23] X. Zhao, G. Zhang, L. Wang, Q. Xue, The tribological mechanism of mos 2 film under different humidity, Tribology Letters 65 (2) (2017) 64.

[24] T. Kubart, T. Polcar, L. Kopeckỳ, R. Novak, D. Novakova, Temperature dependence of tribological properties of mos2 and mose2 coatings, Surface and Coatings Technology 193 (1-3) (2005) 230–233.

[25] N. Renevier, J. Hamphire, V. Fox, J. Witts, T. Allen, D. Teer, Advantages of using self-lubricating, hard, wear-resistant mos2-based coatings, Surface and Coatings Technology 142 (2001) 67–77.

[26] A. Taylor, H. Sinclair, On the determination of lattice parameters by the debye-scherrer method, Proceedings of the Physical Society (1926-1948) 57 (2) (1945) 126.

[27] K. Liang, R. Chianelli, F. Chien, S. Moss, Structure of poorly crystalline mos2—a modeling study, Journal of non-crystalline solids 79 (3) (1986) 251–273.

[28] J. Kauzlarich, J. Williams, Archard wear and component geometry, Proceedings of the Institution of Mechanical Engineers, Part J: Journal of Engineering Tribology 215 (4) (2001) 387–403.

[29] G. Colas, A. Saulot, N. Bouscharain, C. Godeau, Y. Michel, Y. Berthier, How far does contamination help dry lubrication efficiency?, Tribology International 65 (2013) 177–189.

[30] P. Serles, H. Sun, G. Colas, J. Tam, E. Nicholson, G. Wang, J. Howe, A. Saulot, C. V. Singh, T. Filleter, Structure-dependent wear and shear mechanics of nanostructured mos2 coatings, Advanced Materials Interfaces 7 (14) (2020) 1901870.

[31] W. M. Parkin, A. Balan, L. Liang, P. M. Das, M. Lamparski, C. H. Naylor, J. A. Rodríguez-Manzo, A. C. Johnson, V. Meunier, M. Drndic, Raman shifts in electron-irradiated monolayer mos2, ACS nano 10 (4) (2016) 4134–4142.

[32] S. Mignuzzi, A. J. Pollard, N. Bonini, B. Brennan, I. S. Gilmore, M. A. Pimenta, D. Richards, D. Roy, Effect of disorder on raman scattering of single-layer mo s 2, Physical Review B 91 (19) (2015) 195411.

[33] K. Holmberg, H. Ronkainen, A. Laukkanen, K. Wallin, S. Hogmark, S. Jacobson, U. Wiklund, R. M. Souza, P. Ståhle, Residual stresses in tin, dlc and mos2 coated surfaces with regard to their tribological fracture behaviour, Wear 267 (12) (2009) 2142–2156.

[34] G. Levita, P. Restuccia, M. C. Righi, Graphene and mos2 interacting with water: A comparison by ab initio calculations, Carbon 107 (2016) 878–884.

[35] J. R. Lince, M. R. Hilton, A. S. Bommannavar, Exafs of sputter-deposited mos2 films, Thin Solid Films 264 (1) (1995) 120–134.

[36] P. Ehni, I. Singer, Electron-beam micropobe analysis of the wear behavior of sputter-deposited mos2 coatings, Applied surface science 59 (1) (1992) 45–53.

[37] S. Fayeulle, P. Ehni, I. Singer, Paper v (ii) role of transfer films in wear of mos2 coatings, in: Tribology series, Vol. 17, Elsevier, 1990, pp. 129–138.

[38] I. Singer, A thermochemical model for analyzing low wear-rate materials, Surface and Coatings Technology 49 (1-3) (1991) 474–481.

[39] B. Vierneusel, S. Tremmel, S. Wartzack, Effects of deposition parameters on hardness and lubrication properties of thin mos2 films, Materialwissenschaft und Werkstofftechnik 43 (12) (2012) 1029–1035.

[40] G. S. Jung, S. Wang, Z. Qin, F. J. Martin-Martinez, J. H. Warner, M. J. Buehler, Interlocking friction governs the mechanical fracture of bilayer mos2, ACS nano 12 (4) (2018) 3600–3608.

[41] K. Wahl, D. Dunn, I. Singer, Effects of ion implantation on microstructure, endurance and wear behavior of ibad mos2, Wear 237 (1) (2000) 1–11.

[42] J.-M. Martin, Superlubricity of molybdenum disulfide, in: Superlubricity, Elsevier, 2007, pp. 207–225.

[43] R. S. Colbert, W. G. Sawyer, Thermal dependence of the wear of molybdenum disulphide coatings, Wear 269 (11-12) (2010) 719–723.

[44] T. Scharf, R. Goeke, P. Kotula, S. Prasad, Synthesis of au–mos2 nanocomposites: Thermal and friction-induced changes to the structure, ACS applied materials & interfaces 5 (22) (2013) 11762–11767.

[45] X. Li, B. Wang, X. Shu, D. Wang, G. Xu, X. Zhang, J. Lv, Y. Wu, An amorphous mos x modified gc 3 n 4 composite for efficient photocatalytic hydrogen evolution under visible light, RSC advances 9 (28) (2019) 15900–15909.

[46] T. Spalvins, Lubrication with sputtered mos 2 films: principles, operation, and limitations, Journal of Materials Engineering and Performance 1 (3) (1992) 347–351.

[47] Z. Yang, S. Bhowmick, F. G. Sen, A. T. Alpas, Microscopic and atomistic mechanisms of sliding friction of mos2: Effects of undissociated and dissociated h2o, Applied Surface Science (2021) 150270.

[48] H. Nan, Z. Wang, W. Wang, Z. Liang, Y. Lu, Q. Chen, D. He, P. Tan, F. Miao, X. Wang, et al., Strong photoluminescence enhancement of mos2 through defect engineering and oxygen bonding, ACS nano 8 (6) (2014) 5738–5745.